PERFORMANCE ANALYSIS OF QUANTIFYING FLUORESCENCE OF TARGET-CAPTURED MICROPARTICLES FROM MICROSCOPY IMAGES[†] [‡]

Pinaki Sarder Arye Nehorai
Department of Electrical and Systems Engineering
Campus Box 1127, One Brookings Drive
St. Louis, Missouri: 63130-4899, USA

Abstract— **Fluorescence microscopy imaging is widely used in biomedical research, astronomical speckle imaging, remote sensing, positron-emission tomography, and many other applications. In companion papers [1] and [2], we developed a maximum likelihood (ML)–based image deconvolution technique to quantify fluorescence signals from a three-dimensional (3D) image of a target captured microparticle ensemble. We assumed both the additive Gaussian and Poisson statistics for the noise. Imaging is performed by using a confocal fluorescence microscope system. Potential application of microarray technology includes security, environmental monitoring, analyzing assays for DNA or protein targets, functional genomics, and drug development. We proposed a new parametric model of the fluorescence microscope 3D point-spread function (PSF) in terms of basis functions. In this paper, we present a performance analysis of the ML–based deconvolution techniques [1], [2] for both the noise models.**

I. PROBLEM DESCRIPTION

In micro total analysis systems, quantum-dot (q-dot) encoded microparticles, coated with capture reagents, are immobilized in an array. A single array spot contains a large number of microparticles, each of which binds the capture reagent's specific fluorescently labeled bio-target, signified by the different colors in Fig.1. Targets flow tangentially across the ensemble and gradually build up on the surface of the microparticles. These microparticles are identified, and then the targets' concentrations are quantified according to the level of the fluorescence signal per microparticle with a computer-controlled epi-fluorescence microscope. In this paper, we focus on the performance analysis of estimating fluorescence signal from each individual microparticle under the assumption that the targets are already identified [1]-[4]. The fluorescence intensity image of the fluorescent layer on each microparticle is 3D shell shaped. Fig.2 shows the synthetic fluorescence intensity image of the meridional sections of two neighboring shells before (Fig.2a) and after (Fig.2b) acquisition. The acquired 3D image suffers from two basic physical limitations. First, fluorescence microscope imaging properties and measurement imperfections distort the original 3D image and reduce the maximum obtainable resolution by the imaging system, thereby restricting the quantitative analysis of the 3D specimen [5]. Second, the photon-limited image recording of the fluorescence microscope leads to Poisson noise. In Fig.2b, we observe that

[†] This work was supported by the National Science Foundation Grant CCR-0330342.

[‡] Corresponding author: Dr. Arye Nehorai (e-mail: nehorai@ese.wustl.edu, phone: (314) 935-7520, fax: (314) 935-7500)

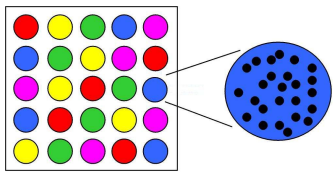

Fig.1. Immobilized particle array, containing 25 spots of microparticles arrayed on a planar surface. Each spot within the array contains microparticles coated with capture reagents.

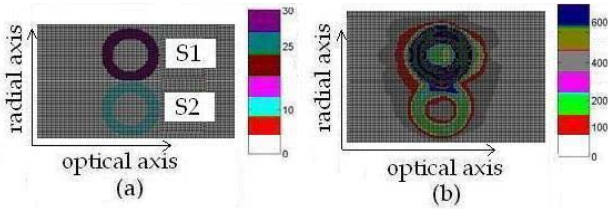

Fig.2. Synthetic fluorescence intensity images of the meridional sections of two neighboring microparticles: (a) before acquiring the image; (b) after acquiring the image.

the intensities of the two neighboring shells S1 and S2 overlap, resulting in a more difficult analysis [1]. In summary, not only does the microscope PSF distort the image of 3D shells in the presence of Poisson noise, but so also do the intensities of neighboring shells merged into each other. In our work, the analysis is local, which justifies the requirement to estimate the center locations of the shells to achieve a satisfactory initialization for the global analysis of the whole ensemble. We present the performance analysis of the developed estimation methods as presented in [1] and [2] for two neighboring shells.

II. FLUORESCENCE MICROSCOPE POINT-SPREAD FUNCTION

Fluorescence microscope 3D PSF is the 3D impulse response of the system and is used to characterize the out-of-focus light. Analytically, the PSF (see, Fig.3) is calculated using the classical (diffraction-based) model of Gibson and Lanni [6], [7], which has two computational limitations: (i) evaluation of its partial derivatives with respect to its parameters is computationally demanding, and (ii) the number of the parameters in it may not be optimal. Fig.3a shows the meridional (x-z) section of a numerically computed PSF of a fluorescence microscope. We can see that most of the energy of the PSF is concentrated near its point of origin, represented by a Gaussian peak. Smaller Gaussian peaks appear along the optical axis

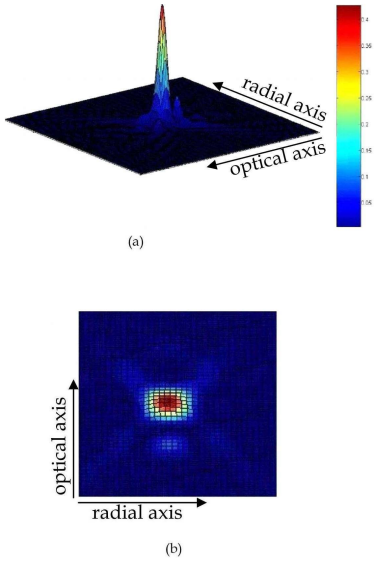

Fig.3. (a) Meridional section of the numerically computed PSF of a fluorescence microscope with the signal intensity represented by height; (b) projected top view of the signal intensity of the PSF in the meridional section.

which distinguishes the meridional[1] profile of the PSF from the conventional "X" shape [8]. The tails of the PSF in Fig.3b resemble the diffraction ring patterns of the 3D PSF. Note that the insignificant tails are not visible in Fig.3a. In [1] and [2], we constructed a parametric model of the fluorescence microscope PSF in terms of basis functions that approximates the complex PSF model of Gibson and Lanni in the least-squares sense [1], [2]. Assuming radial symmetry, our model is given by

$$h(x,y,z;\boldsymbol{\theta}) = a_1 \exp\left(-\frac{1}{2}\left(\frac{z^2}{{\sigma_1}^2}+\frac{(x^2+y^2)}{{\sigma_2}^2}\right)\right)$$
$$+a_2\exp\left(-\frac{1}{2}\left(\frac{(z-\mu_1)^2}{{\sigma_3}^2}+\frac{(x^2+y^2)}{{\sigma_2}^2}\right)\right)+\sum_{i=1}^{4}(c_{\mathrm{a}_i}$$
$$-m_{\mathrm{a}_i}(\sqrt{x^2+y^2}-r_0))\exp\left(-\frac{1}{2}\left(\frac{(z+m_{\mathrm{m}_i}(\sqrt{x^2+y^2})-c_{\mathrm{m}_i})^2}{{\sigma_4}^2}\right)\right)$$
$$u((\sqrt{x^2+y^2})-r_0)u(r_0), \qquad (1)$$

where $\boldsymbol{\theta} = [\sigma_1,\sigma_2,\sigma_3,\sigma_4,\mu_1,r_0,m_{\mathrm{m}_1},m_{\mathrm{m}_2},m_{\mathrm{m}_3},m_{\mathrm{m}_4},c_{\mathrm{m}_1},c_{\mathrm{m}_2},c_{\mathrm{m}_3},c_{\mathrm{m}_4},a_1,a_2,c_{\mathrm{a}_1},c_{\mathrm{a}_2},c_{\mathrm{a}_3},c_{\mathrm{a}_4},m_{\mathrm{a}_1},m_{\mathrm{a}_2},m_{\mathrm{a}_3},m_{\mathrm{a}_4}]^T$ is the unknown parameter vector, $u(\cdot)$ the unit step function, and $[\cdot]^T$ the matrix transpose operation. The model (1) reduces the number of unknowns from thousands of pixel values to a smaller finite number of parameters. The first term of $h(x,y,z;\boldsymbol{\theta})$ in (1) approximates the PSF's central bigger lobe. Similarly, the second term approximates the shifted smaller lobe along the optical axis. The terms inside the summation in (1) model the significant tails of the PSF along the radial and optical directions with a linear approximation of amplitudes. Our simple model not only transfers the Gibson and Lanni's physical model [7] to a pure mathematical model but also reduces the number of unknowns from thousands of voxel[2] values to a smaller finite numbers of parameters. Additionally, computation of the partial derivatives of (1) with respect to elements in $\boldsymbol{\theta}$ is also simplified. We impose a positivity constraint in (1) when evaluating the estimation algorithm using MATLAB.

In our research [1], [2], we estimate the intensity ratios and centers of the shells to quantify their fluorescence levels using the parametric PSF model (1). We assume both the additive Gaussian and Poisson statistics for the noise.

III. MEASUREMENT MODEL

Physical model: Assuming isoplanatism, the fluorescence microscope is modeled as a linear shift–invariant system, due to the incoherent nature of the emitted fluorescent light [9]. In that case the 3D image is represented by the convolution operation between the PSF $h(x,y,z)$ of the fluorescence microscope system and the 3D object of interest $f(x,y,z)$. The imaging process can be expressed analytically [10] as

$$g(x,y,z) = h(x,y,z)\otimes f(x,y,z), \qquad x,y,z\in\mathbb{R}, \qquad (2)$$

where $g(x,y,z)$ is the measured data and $\otimes$ the convolution operation.

Statistical models: In practice, the photon-limited image recording of the fluorescence microscope leads to Poisson noise [9]. Although the Poisson statistics provide a realistic noise model [11], in some applications an additive Gaussian noise model is assumed, due to its numerical advantages during analysis.

1) *Poisson model:* The quantum nature of light leads to a Poisson modeling as follows:

$$\beta g(x,y,z) = \mathcal{P}(\beta[h(x,y,z)\otimes f(x,y,z)])+\mathcal{P}(\beta[b(x,y,z)]), \qquad (3)$$

where β is the reciprocal of the photon-conversion factor, $\beta g(x,y,z)$ the number of photons measured in the detector, $\mathcal{P}$ a Poisson process, and $b(x,y,z)$ the background signal. For fluorescence microscopy the photon-conversion factor is proportional to several physical parameters, such as the integration time and the quantum efficiency of the detector [12]. Both $\mathcal{P}(\beta[h(x,y,z)\otimes f(x,y,z)])$ and $\mathcal{P}(\beta[b(x,y,z)])$ are independent Poisson random variables, and hence the measured output is a Poisson random variable $\mathcal{P}(\beta[h(x,y,z)\otimes f(x,y,z)+b(x,y,z)])$.

2) *Gaussian model:* The additive Gaussian noise model is given by

$$g(x,y,z) = h(x,y,z)\otimes f(x,y,z)+w(x,y,z), \quad x,y,z\in\mathbb{R}, \qquad (4)$$

where $w(x,y,z)$ is an additive Gaussian noise. Note that the background term is not modeled in the additive Gaussian noise model, because it can be estimated and then removed from

[1]The meridional section is defined as a plane along the optical axis (perpendicular to the plane of focus) passing through the origin.

[2]A 3D image pixel.

the acquired image before the deconvolution operation. For the Poisson noise model, this term cannot be incorporated in a term that is independent of $(h(x,y,z) \otimes f(x,y,z))$ and thus needs to be taken into account explicitly.

Under low SNR, the additive Gaussian noise model provides a poorer description of the fluorescence microscopy imaging than the Poisson model [5]. With the high SNR, the Gaussian noise model performs satisfactorily by employing the central limit theorem [11] for a large number of measurement data. It has been widely claimed in the literature that the deconvolution performance of the additive Gaussian noise model is inferior to the correct Poisson noise model.

IV. ESTIMATION

The parametric forms of two neighboring shells S1 and S2 are given by

$$s_1(x,y,z;m,x_{\mathrm{c}_1},y_{\mathrm{c}_1},z_{\mathrm{c}_1}) = \begin{cases} m & \text{if } r_1 \le \sqrt{(x-x_{\mathrm{c}_1})^2+(y-y_{\mathrm{c}_1})^2+(z-z_{\mathrm{c}_1})^2} \le r_2, \\ 0 & \text{otherwise,} \end{cases} \tag{5}$$

$$s_2(x,y,z;m,r,x_{\mathrm{c}_2},y_{\mathrm{c}_2},z_{\mathrm{c}_2}) = \begin{cases} mr & \text{if } r_1 \le \sqrt{(x-x_{\mathrm{c}_2})^2+(y-y_{\mathrm{c}_2})^2+(z-z_{\mathrm{c}_2})^2} \le r_2, \\ 0 & \text{otherwise,} \end{cases} \tag{6}$$

where the two shells' unknown centers are $(x_{\mathrm{c}_1},y_{\mathrm{c}_1},z_{\mathrm{c}_1})$ and $(x_{\mathrm{c}_2},y_{\mathrm{c}_2},z_{\mathrm{c}_2})$, and the unknown fluorescence intensity levels are m and mr with an unknown intensity ratio r. The known inner and outer radii of $s_{(\cdot)}(\cdot)$ are r_1 and r_2 and the principal parameters of interest are $m, r, x_{\mathrm{c}_1}, y_{\mathrm{c}_1}, z_{\mathrm{c}_1}, x_{\mathrm{c}_2}, y_{\mathrm{c}_2}$, and z_{c_2}. We redefine,

$$o(x,y,z;r,x_{\mathrm{c}_1},y_{\mathrm{c}_1},z_{\mathrm{c}_1},x_{\mathrm{c}_2},y_{\mathrm{c}_2},z_{\mathrm{c}_2}) = \begin{cases} 1 & \text{if } r_1 \le \sqrt{(x-x_{\mathrm{c}_1})^2+(y-y_{\mathrm{c}_1})^2+(z-z_{\mathrm{c}_1})^2} \le r_2, \\ r & \text{if } r_1 \le \sqrt{(x-x_{\mathrm{c}_2})^2+(y-y_{\mathrm{c}_2})^2+(z-z_{\mathrm{c}_2})^2} \le r_2, \\ 0 & \text{otherwise.} \end{cases} \tag{7}$$

Hence, after the convolution operation we obtain

$$\begin{aligned} &h(x,y,z;\boldsymbol{\theta}) \otimes [s_1(x,y,z;m,x_{\mathrm{c}_1},y_{\mathrm{c}_1},z_{\mathrm{c}_1}) + \\ &s_2(x,y,z;m,r,x_{\mathrm{c}_2},y_{\mathrm{c}_2},z_{\mathrm{c}_2})] = \\ &ma_1\left[\exp\left(-\tfrac{1}{2}\left(\tfrac{z^2}{{\sigma_1}^2}+\tfrac{(x^2+y^2)}{{\sigma_2}^2}\right)\right)\otimes o(\cdot)\right] + \\ &ma_2\left[\exp\left(-\tfrac{1}{2}\left(\tfrac{(z-\mu_1)^2}{{\sigma_3}^2}+\tfrac{(x^2+y^2)}{{\sigma_2}^2}\right)\right)\otimes o(\cdot)\right] \\ &+\textstyle\sum_{i=1}^{4} m(c_{\mathrm{a_i}} - m_{\mathrm{a_i}}((\sqrt{x^2+y^2})-r_0)) \\ &\left[\exp\left(-\tfrac{1}{2}\left(\tfrac{(z+m_{\mathrm{m_i}}(\sqrt{x^2+y^2})-c_{\mathrm{m_i}})^2}{{\sigma_4}^2}\right)\right)\right. \\ &\left.u((\sqrt{x^2+y^2})-r_0)u(r_0)\otimes o(\cdot)\right]. \end{aligned} \tag{8}$$

The available measurements are $\{g(x,y,z), 1{\le}x{\le}L, 1{\le}y{\le}P, 1{\le}z{\le}K\}$.

Estimation under Gaussian noise: The noise $w(x,y,z)$ is assumed to be additive independent from voxel to voxel, Gaussian distributed with zero mean and unknown variance ${\sigma_e}^2$. For convenience, we define $\boldsymbol{\varphi} = [x_{\mathrm{c}_1}, y_{\mathrm{c}_1}, z_{\mathrm{c}_1}, x_{\mathrm{c}_2}, y_{\mathrm{c}_2}, z_{\mathrm{c}_2}, r, \sigma_1, \sigma_2, \sigma_3, \sigma_4, \mu_1, r_0, m_{\mathrm{m}_1}, m_{\mathrm{m}_2}, m_{\mathrm{m}_3}, m_{\mathrm{m}_4}, c_{\mathrm{m}_1}, c_{\mathrm{m}_2}, c_{\mathrm{m}_3}, c_{\mathrm{m}_4}]^T$ and $\boldsymbol{\vartheta} = [a_1, a_2, c_{\mathrm{a}_1}, c_{\mathrm{a}_2}, c_{\mathrm{a}_3}, c_{\mathrm{a}_4}, m_{\mathrm{a}_1}, m_{\mathrm{a}_2}, m_{\mathrm{a}_3}, m_{\mathrm{a}_4}]^T$. With these assumptions and notations we can lump the measurements into vector form: $\boldsymbol{g} = mN(\boldsymbol{\varphi})\boldsymbol{\vartheta} + \boldsymbol{w}$, where $\boldsymbol{g}$ is an $(LPK \times 1)$ dimensional vector whose $(LP(z-1)+L(y-1)+x)$th component is $g(x,y,z)$ and similarly for $\boldsymbol{w}$. The matrix $N(\boldsymbol{\varphi})$ is of dimension $(LPK{\times}10)$ and its $(LP(z-1)+L(y-1)+x)$th row is given by

$$\begin{aligned} &\left[\exp\left(-\tfrac{1}{2}\left(\tfrac{z^2}{{\sigma_1}^2}+\tfrac{(x^2+y^2)}{{\sigma_2}^2}\right)\right)\otimes o(\cdot), \exp\left(-\tfrac{1}{2}\left(\tfrac{(z-\mu_1)^2}{{\sigma_3}^2}+\right.\right.\right. \\ &\left.\left.\left.\tfrac{(x^2+y^2)}{{\sigma_2}^2}\right)\right)\otimes o(\cdot), \exp\left(-\tfrac{1}{2}\left(\tfrac{(z+m_{\mathrm{m}_1}(\sqrt{x^2+y^2})-c_{\mathrm{m}_1})^2}{{\sigma_4}^2}\right)\right) \\ &u((\sqrt{x^2+y^2})-r_0)u(r_0)\otimes o(\cdot), \cdots\cdots\cdots\cdots \\ &\exp\left(-\tfrac{1}{2}\left(\tfrac{(z+m_{\mathrm{m}_4}(\sqrt{x^2+y^2})-c_{\mathrm{m}_4})^2}{{\sigma_4}^2}\right)\right)u((\sqrt{x^2+y^2})-r_0), \\ &u(r_0)\otimes o(\cdot), ((\sqrt{x^2+y^2})-r_0) \\ &\exp\left(-\tfrac{1}{2}\left(\tfrac{(z+m_{\mathrm{m}_1}(\sqrt{x^2+y^2})-c_{\mathrm{m}_1})^2}{{\sigma_4}^2}\right)\right)u((\sqrt{x^2+y^2})-r_0) \\ &u(r_0)\otimes o(\cdot), \cdots\cdots\cdots\cdots ((\sqrt{x^2+y^2})-r_0) \\ &\exp\left(-\tfrac{1}{2}\left(\tfrac{(z+m_{\mathrm{m}_1}(\sqrt{x^2+y^2})-c_{\mathrm{m}_1})^2}{{\sigma_4}^2}\right)\right) \\ &\left.u((\sqrt{x^2+y^2})-r_0)u(r_0)\otimes o(\cdot)\right]^T. \end{aligned} \tag{9}$$

The ML estimate of the parameters (see, e.g., [1]) is

$$\hat{\boldsymbol{\varphi}} = \operatorname{argmax}\{\boldsymbol{g}^T P_N(\boldsymbol{\varphi})\boldsymbol{g}\}, \tag{10}$$

$$\widehat{m\boldsymbol{\vartheta}} = [N^T(\hat{\boldsymbol{\varphi}})N(\hat{\boldsymbol{\varphi}})]^{-1}N^T(\hat{\boldsymbol{\varphi}})\boldsymbol{g}, \tag{11}$$

$${\hat{\sigma_e}}^2 = (LPK)^{-1}\boldsymbol{g}^T P_N^{\perp}(\hat{\boldsymbol{\varphi}})\boldsymbol{g}, \tag{12}$$

where $P_N(\boldsymbol{\varphi})$ is the projection matrix on the column space of $N(\boldsymbol{\varphi})$ [13], and ${P^{\perp}}_N(\hat{\boldsymbol{\varphi}})$ the complementary projection matrix, given by

$$\begin{aligned} P_N(\boldsymbol{\varphi}) &= N(\boldsymbol{\varphi})[N^T(\boldsymbol{\varphi})N(\boldsymbol{\varphi})]^{-1}N^T(\boldsymbol{\varphi}) \\ P_N^{\perp}(\boldsymbol{\varphi}) &= I - P_N(\boldsymbol{\varphi}). \end{aligned} \tag{13}$$

Estimation under Poisson noise: We evaluate the analysis using the noise model (3), where the noise is assumed to be

independent from voxel to voxel. The unknown background intensity is assumed to be constant as $\{b(x,y,z)=\tau\ \forall\ x,y,z\in\mathbb{R}\}$. We define

$$i(x,y,z;\boldsymbol{\varphi},m\boldsymbol{\vartheta})=h(x,y,z;\boldsymbol{\theta})\otimes s(x,y,z;m,x_{c_1},y_{c_1},z_{c_1}). \tag{14}$$

We lump the measurement intensity values $g(x,y,z)$ into vector form for each co-ordinate (x,y,z) as

$$\boldsymbol{g}=\boldsymbol{\mathcal{P}}(\boldsymbol{i}(\boldsymbol{\upsilon})+\tau\mathbf{1}), \tag{15}$$

where $\boldsymbol{\mathcal{P}}(\cdot)$ is a vector whose element is a Poisson random variable $\mathcal{P}(\cdot)$, $\boldsymbol{\upsilon}=[\boldsymbol{\varphi}^T,m\boldsymbol{\vartheta}^T]^T$, $\boldsymbol{i}(\boldsymbol{\upsilon})$ an $(LPK\times 1)$–dimensional vector whose $(LP(z-1)+L(y-1)+x)$th component is $i(x,y,z;\boldsymbol{\varphi},m\boldsymbol{\vartheta})$, and $\mathbf{1}$ an $(LPK\times 1)$–dimensional vector of elements 1. We maximize the log-likelihood function

$$J(\boldsymbol{\alpha})=\boldsymbol{g}^T\ln(\boldsymbol{i}(\boldsymbol{\upsilon})+\tau\mathbf{1})-\mathbf{1}^T(\boldsymbol{i}(\boldsymbol{\upsilon})+\tau\mathbf{1}) \tag{16}$$

to obtain the ML estimate of the unknown parameters where $\boldsymbol{\alpha}=[\boldsymbol{\upsilon}^T,\tau]^T$ is the parameter vector [2]. A detailed derivation of (16) from (3) is provided in [2].

V. PERFORMANCE BOUND ANALYSIS

In our research, we choose the Craḿer-Rao bound (CRB) as a performance measure [1], [2]. CRB is the lowest bound on the variance of any unbiased estimator under certain regularity conditions with the important features of being *universal*, i.e., independent of the algorithm used for estimation among the unbiased ones, and *asymptotically tight*, meaning that for certain distributions, there exist algorithms that achieve the bound as the number of samples become large. Note that the estimate achieves the CRB asymptotically. In brief, the CRB is a performance measure that may be useful for determining the best accuracy we can expect for a certain algorithm. In our research, we obtain satisfactory CRBs on the variance of unknown parameters.

Performance under Gaussian noise: We define as the parameter vector, $\boldsymbol{\mu}(\boldsymbol{g})=mN(\boldsymbol{\varphi})\boldsymbol{\vartheta}$ the mean of the measurement vector $\boldsymbol{g}$, and L the Fisher information matrix of dimension (31×31) with the (i,k)th entry $\{L_{i,k},1\le i\le 31,1\le k\le 31\}$ given as

$$L_{i,k}=\frac{1}{{\sigma_e}^2}\big[\frac{\partial}{\partial\boldsymbol{\upsilon}_i}(\boldsymbol{\mu}(\boldsymbol{g}))\big]^T\big[\frac{\partial}{\partial\boldsymbol{\upsilon}_k}(\boldsymbol{\mu}(\boldsymbol{g}))\big], \tag{17}$$

where $\boldsymbol{\upsilon}_i$ is the ith element of the parameter vector $\boldsymbol{\upsilon}$. The CRB for the unbiased estimates of the parameters in $\boldsymbol{\upsilon}$ is derived from the diagonal elements of the matrix L^{-1} [13].

Performance under Poisson noise: The Fisher information matrix L is a (32×32) matrix with (i,k)th entry $\{L_{i,k},1\le i\le 32,1\le k\le 32\}$ as

$$L_{i,k}=\beta\Big[\frac{\partial}{\partial\boldsymbol{\alpha}_i}(\boldsymbol{i}(\boldsymbol{\upsilon})+\tau\mathbf{1})\Big]^T\Big[\frac{\frac{\partial}{\partial\boldsymbol{\alpha}_k}(\boldsymbol{i}(\boldsymbol{\upsilon})+\tau\mathbf{1})}{(\boldsymbol{i}(\boldsymbol{\upsilon})+\tau\mathbf{1})}\Big], \tag{18}$$

where the division of vectors is performed element to element, $\boldsymbol{\alpha}_i$ is the ith element of the parameter vector $\boldsymbol{\alpha}$. The derivation of (18) is provided in the following.

Proof: From (16) we have

$$\frac{\partial}{\partial\alpha_j}\log(p(\beta g(\cdot);x,y,z\in\mathbb{R}))=\beta\Big[\sum_{x,y,z\in\mathbb{R}}\Big\{\frac{g(\cdot)\frac{\partial}{\partial\alpha_j}(h(\cdot)\otimes f(\cdot)+b(\cdot))}{(h(\cdot)\otimes f(\cdot)+b(\cdot))}-\frac{\partial}{\partial\alpha_j}(h(\cdot)\otimes f(\cdot)+b(\cdot))\Big\}\Big]. \tag{19}$$

Hence,

$$\frac{\partial^2}{\partial\alpha_i\alpha_j}\log(p(\beta g(\cdot);x,y,z\in\mathbb{R}))=\beta\Big[\sum_{x,y,z\in\mathbb{R}}\Big\{\frac{g(\cdot)\frac{\partial^2}{\partial\alpha_i\alpha_j}(h(\cdot)\otimes f(\cdot)+b(\cdot))}{(h(\cdot)\otimes f(\cdot)+b(\cdot))}-\frac{g(\cdot)\frac{\partial}{\partial\alpha_i}(h(\cdot)\otimes f(\cdot)+b(\cdot))\frac{\partial}{\partial\alpha_j}(h(\cdot)\otimes f(\cdot)+b(\cdot))}{(h(\cdot)\otimes f(\cdot)+b(\cdot))^2}$$
$$-\frac{\partial^2}{\partial\alpha_i\alpha_j}(h(\cdot)\otimes f(\cdot)+b(\cdot))\Big\}\Big]. \tag{20}$$

Since $\mathrm{E}[g(\cdot)]=(h(\cdot)\otimes f(\cdot)+b(\cdot))$, where $\mathrm{E}[\cdot]$ denotes an expectation operation, we obtain from (20)

$$-E\big[\frac{\partial^2}{\partial\alpha_i\alpha_j}\log(p(\beta g(\cdot);x,y,z\in\mathbb{R}))\big]=\beta\Big[\sum_{x,y,z\in\mathbb{R}}\frac{\frac{\partial}{\partial\alpha_i}(h(\cdot)\otimes f(\cdot)+b(\cdot))\frac{\partial}{\partial\alpha_j}(h(\cdot)\otimes f(\cdot)+b(\cdot))}{(h(\cdot)\otimes f(\cdot)+b(\cdot))}\Big]. \tag{21}$$

Therefore $\{L_{i,k},1\le i\le 28,1\le k\le 28\}$ is given by,

$$L_{i,k}=\beta\Big[\frac{\partial}{\partial\boldsymbol{\alpha}_i}(\boldsymbol{i}(\boldsymbol{\upsilon})+\tau\mathbf{1})\Big]^T\Big[\frac{\frac{\partial}{\partial\boldsymbol{\alpha}_k}(\boldsymbol{i}(\boldsymbol{\upsilon})+\tau\mathbf{1})}{(\boldsymbol{i}(\boldsymbol{\upsilon})+\tau\mathbf{1})}\Big]. \tag{22}$$

VI. NUMERICAL EXAMPLES

Two neighboring spherical shell-like objects (shells S1 and S2 in Fig.10) are generated on a $129\times 129\times 129$ sampling lattice, with a sampling interval of 0.179μm along the X,Y, and Z directions. Each shell has a diameter of 4.3μm and a thickness of 1.43μm, respectively, and the distance between their centers is 7.16μm. The maximum intensities of the shells

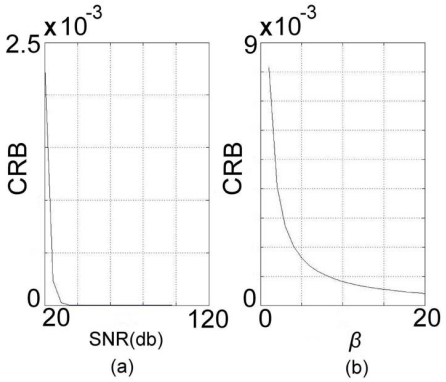

Fig.4. Craḿer-Rao bound on the relative intensity r of shells S1 and S2 as a function of SNR and β for the: (a) additive Gaussian noise model, and (b) Poisson noise model, respectively.

are 10 and 30, respectively. The simulated confocal images are obtained by convolving the object with a calculated PSF using (1). For the model (1), we use these parameters: ${\sigma_1}^2 = 6.7$, ${\sigma_2}^2 = 5.7$, ${\sigma_3}^2 = 3.36$, ${\sigma_4}^2 = 10.92$, $\mu_1 = 11.29$, $r_0 = 1$, $m_{\mathrm{m}_1} = 2.0262$, $m_{\mathrm{m}_2} = 0.8465$, $m_{\mathrm{m}_3} = -1.3135$, $m_{\mathrm{m}_4} = 0$, $c_{\mathrm{m}_1} = 5.44$, $c_{\mathrm{m}_2} = 0.9727$, $c_{\mathrm{m}_3} = -1.6$, $c_{\mathrm{m}_4} = 0.0362$, $a_1 = 0.4273$, $a_2 = 0.09$, $c_{\mathrm{a}_1} = 0.0221$, $c_{\mathrm{a}_2} = 0.0103$, $c_{\mathrm{a}_3} = 0.0151$, $c_{\mathrm{a}_4} = 0.0011$, $m_{\mathrm{a}_1} = 0.0009$, $m_{\mathrm{a}_2} = 0.0002$, $m_{\mathrm{a}_3} = 0.0004$, $m_{\mathrm{a}_4} = 0$. The background signal intensity is assumed to be 0. Additive Gaussian or Poisson noise of varying levels was generated in the image. For the Gaussian noise we define a SNR as

$$\mathrm{SNR} = \frac{\max_i (h(\cdot) \otimes f(\cdot))_i - \min_i (h(\cdot) \otimes f(\cdot))_i}{\sigma_e}. \qquad (23)$$

For the Poisson statistics, the noise is completely characterized by the photon conversion factor $\frac{1}{\beta}$. In our simulations we choose the mean of the Poisson process equal to $\beta(h(\cdot) \otimes f(\cdot) + b(\cdot))$; thus the number of detected photons is proportional to β. As a consequence, we choose β as a SNR measure for the Poisson statistics. In Fig.4a and 4b, we plot the CRB of the relative intensity r of shells S1 and S2 as a function of SNR and β for the additive Gaussian and Poisson noise statistics, respectively [1], [2]. In Fig.5a and 5b, we compare the CRB and mean-square error (MSE) of the estimated yc1 of S1 as a function of SNR under Gaussian and Poisson noise, respectively. We observe that the MSE of the estimated yc1 is closer to its CRB for high SNR and deviates significantly for lower SNR.

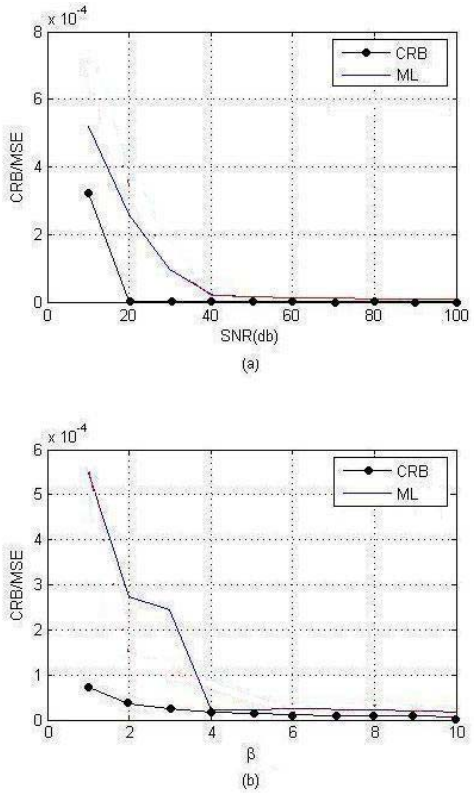

Fig.5. Craḿer-Rao bound and mean-square error of the estimated y_{c_1} as a function of SNR for the: (a) additive Gaussian noise model, and (b) Poisson noise model, respectively.

VII. CONCLUSION

In this summary, we addressed the performance bound analysis for quantifying fluorescence signals of q-dot–encoded microparticles using the CRB analysis. An analysis-based performance measure such as CRB is necessary [14] in our application, since the goal of deconvolution is to improve the quantitative analysis of the fluorescence microscopy images. For both noise models, a lower value of CRB in the higher SNR regions signifies that the MSE of the estimated parameters can get closer to the CRB value for high SNR, using a ML–based image deconvolution technique for deconvolving of 3D fluorescence microscopy images [1], [2].

REFERENCES

[1] P. Sarder and A. Nehorai, "Quantifying fluorescence of target-captured microparticles from microscopy images in Gaussian noise using maximum likelihood estimation," unpublished.

[2] P. Sarder and A. Nehorai, "Estimating fluorescence of target-captured microparticles from microscopy images in Poisson noise," unpublished.

[3] P. W. Stevens, C. H. J. Wang, and D. M. Kelso, "Immobilized particle arrays: Coalescence of planar and suspension-array technologies," *Anal. Chem.*, vol. 75, pp. 1141-1146, 2003.

[4] P. W. Stevens and D. M. Kelso, "Imaging and analysis of immobilized particle arrays," *Anal. Chem.*, vol. 75, pp. 1147-1154, 2003.

[5] G. M. P. van der Kempen, L. J. van Vliet, P. J. Verveer, and H. T. M. van der Voort, "A quantitative comparison of image restoration methods for confocal microscopy," *J. Microsc.*, vol. 185, no. 3, pp. 354-365, 1997.

[6] J. Markham and J. Conchello, "Parametric blind deconvolution: A robust method for the simultaneous estimation of image and blur," *J. Opt. Soc. Am. A.,* vol. 16, pp. 2377-2391, 1999.

[7] S. F. Gibson and F. Lanni, "Experimental test of an analytical model of aberration in an oil-immersion objective lens used in three-dimensional light microscopy,"*J. Opt. Soc. Am. A.,* vol. 8, pp. 1601-1612, 1991.

[8] J. G. McNally, T. Karpova, J. Cooper, and J. A. Conchello, "Three-dimensional imaging by deconvolution microscopy," *Methods,* vol. 19, no. 3, pp. 373-385, 1999.

[9] M. P. van Kempen, *Image Restoration in Fluorescence Microscopy,* Ph.D. thesis, Delft Technical University, Delft, The Netherlands, 1999.

[10] D. Kundur and D. Hatzinakos, "Blind image deconvolution," *IEEE Signal Processing Magazine*, vol. 13, No. 3, pp. 43-64, 1996.

[11] D. L. Snyder and M. I. Miller, *Random Point Processes in Time and Space, Second Edition*, New York: Springer-Verlag, 1991.

[12] T. M. Jovin and D. J. Arndt-Jovin, "Luminescence digital imaging microscopy," *Annu. Rev. Biophys. Chem.*, vol. 18, pp. 271-308, 1989.

[13] S. M. Kay, *Fundamentals of Statistical Signal Processing, Estimation Theory*, Englewood Cliffs, New Jersy: PTR Prentice Hall, 1993.

[14] P. Sarder and A. Nehorai, "An overview of deconvolution methods of 3D fluorescence microscopy images," to appear in *IEEE Signal Processing Magazine*.